# HYDROGRAPHIC AND FLOW STRUCTURE IN THE CHESAPEAKE BAY MOUTH AND PLUME REGION UNDER HIGH FRESHWATER DISCHARGE CONDITIONS

Kristine Holderied*

Arnoldo Valle-Levinson

Center for Coastal Physical Oceanography
Old Dominion University
Norfolk, Virginia, USA, 23529

*Corresponding Author: kris@ccpo.odu.edu

Prepared for Continental Shelf Research

November 1997

## ABSTRACT

Hydrographic and horizontal velocity measurements were obtained along three transects in the Chesapeake Bay mouth and plume region in order to characterize the spatial and temporal variability of salinity and flow in this area during a period of high river discharge and moderate wind forcing (3-7 June 1996). All three transects were characterized by a bathymetry consisting of a channel flanked by shoals. Tidal variability of the salinity and flow was dominated by the semidiurnal constituents, but contributions from the diurnal constituents were significant. Intratidal features included sharpening of the pycnocline in the channel after maximum ebb currents, due to tidal straining, and development of surface fronts over the channel shoulders, due to horizontal velocity convergence. Away from the bay mouth, intratidal observations indicated that the cross-shore movement of the low-salinity plume was controlled by direct wind forcing. However, both at the mouth and offshore, the subtidal, low-salinity core of the outflow plume was consistently located over the deep channel, reflecting the influence of bathymetry and inertial forces on subtidal circulation, and the dominance of gravitational forcing over the channel. Subtidal velocity data suggested the presence of a surface anticyclonic gyre at the northern portion of the bay entrance and a second anticylonic gyre south of the bay mouth, formed as the plume separated from the coast before turning southward. Subtidal horizontal velocity convergence of order $10^{-4}$ $s^{-1}$ was consistently observed over the shoulders of the channel, produced by differences in the vertical structure of the flow over the shoals and in the channel. For the first time, subtidal salinity and flow fields were measured at sufficient spatial resolution to estimate the net, normalized salinity transport across the Chesapeake Bay mouth, which was calculated to be $1.36 \times 10^4$ $m^3/s$ into the estuary.

## INTRODUCTION

The study of interactions between estuarine and continental shelf circulations is crucial to understanding the fate of nutrients, pollutants and larvae transported between the estuary and the shelf. The exchange of water between the estuary and the ocean is complicated by the presence of multiple forcing mechanisms, including tides, freshwater runoff, winds, and barometric pressure. Bathymetry interacts with these mechanisms to modify the flow patterns. The typically shallow areas of the lower part of a coastal plain estuary and of the near coastal region allow for relatively rapid responses of circulation to changes in the local wind forcing. This rapid response, along with a typically large influence from the tides, results in circulation patterns that shift rapidly on time scales of a few hours.

The Chesapeake Bay is one example of a relatively wide coastal plain estuary with freshwater input from extensive river runoff over a large watershed. Circulation in the bay mouth and outflow region is significantly influenced by both buoyancy and tidal forcing, and depths in this region are shallow enough that local wind forcing is important. Several studies have shown the response of the density (Boicourt, 1981; Boicourt, *et al.*, 1987; Paraso and Valle-Levinson, 1996) and flow (Valle-Levinson and Lwiza, submitted) fields in the Chesapeake Bay plume to changes in the wind field. Northeasterly (onshore) winds have been shown to increase subtidal water elevations at the bay mouth and confine the plume tightly to the southern part of the estuary and along the coast to the south of the bay mouth. Conversely, southwesterly (offshore) winds reduce subtidal water elevations at the bay mouth and allow the plume to move further offshore before turning south along the coast. The semidiurnal tidal constituent dominates tidal forcing in the lower Chesapeake Bay, with interaction between the $M_2$, $N_2$, and $S_2$ constituents causing fortnightly and monthly tidal variability (Browne and Fisher, 1988). A distinct difference emerges between successive spring (or neap) tides, creating primary and secondary spring (and neap) tides within one month.

Our understanding of the effects of these forcing mechanisms on the Chesapeake Bay estuarine-coastal circulation has come primarily from information collected with moored instruments, with only limited spatial resolution. Recent measurements with a towed acoustic Doppler current profiler (ADCP) have provided much better spatial resolution of the flow field (Valle-Levinson and Lwiza, submitted), but only limited temporal resolution. Even with these limitations, such studies have illustrated the strong spatial and temporal variability, at relatively small scales, in this region. In order to describe and understand this variability, there is a need for basic hydrographic and current data, at the spatial scales of local bathymetric features and the temporal scales of tidal variability.

The objective of this study is to describe the hydrographic structure and flow field in the Chesapeake Bay outflow region during a period of moderate winds and high freshwater discharge. The detailed observations of the salinity and current fields in this study will facilitate interpretation of future ADCP current measurements obtained in the same region by different research programs. The observations will also help validate models of the Chesapeake Bay mouth and outflow region. It is intended that these observations will be compared to data from future studies in the region, under different wind and density forcing conditions.

## DATA COLLECTION AND PROCESSING

Three transects (Figure 1) were surveyed from June 3 to 7, 1996, onboard the United States National Oceanic and Atmospheric Administration (NOAA) ship *Ferrel*. Ten repetitions were made of each transect over three successive, 25-hour periods. Using an Applied Microsystems EMP-2000 Conductivity-Temperature-Depth (CTD) recorder and current meter, vertical stations were occupied at approximately 1.8 km intervals along each transect. The CTD/current meter assembly was held for five seconds at approximately 0.5 meter depth intervals to accomodate the response time of the current meter, which had an accuracy of 0.015 m/s. The 25-hour sampling period facilitated separation of tidal and subtidal contributions from the observations. On June 3 and 4, ten stations were occupied along Transect 3, extending offshore 16.8 km to the east-northeast from Virginia Beach. On June 4 and 5, eleven stations were occupied along Transect 2, extending offshore 18.3 km to the northeast from Virginia Beach. Ten stations along Transect 1, extending 15.9 km across the Chesapeake Bay mouth from Cape Henry to Fishermans Island, were occupied on June 5 and 6. All three transects were approximately perpendicular to Chesapeake Channel and were characterized by a channel/shoals bathymetry. The northern portion of Transect 1 also crossed the shallower North Channel, just south of Fishermans Island.

The current velocity data were rotated to create along-channel (perpendicular to the transect) and across-channel (parallel to the transect) velocity components. The salinity, temperature, density and current velocity data were then interpolated to a grid with 300 m spacing in the horizontal, across-channel (along-transect) direction and 0.5 m in the vertical direction. Contoured hydrographic and flow fields on an across-channel versus depth grid were produced for each repetition of each transect, with data from the end stations used twice on successive repetitions. The buoyant surface water leaving the bay was warmer than the more saline shelf water, so the salinity, temperature and density fields had the same spatial and temporal structure. Only the salinity data are shown and discussed in detail here, with the understanding that they also represent patterns in the temperature and density data.

Wind and atmospheric pressure data were recorded by the ship's anemometer and barometer and also obtained from the southernmost island of the Chesapeake Bay Bridge-Tunnel (CBBT) and from the Chesapeake Light Tower (CLT) (see Figure 1 for locations). Wind observations on the ship and at CLT did not differ significantly from the observations on the CBBT, so only plots of CBBT winds are provided in this paper. Water elevation data were obtained from the CBBT tide gauge. Monthly freshwater discharges to the Chesapeake Bay before and during the study period were obtained from the United States Geological Survey (USGS). These values are calculated as the sum of net discharges measured from each of the major rivers in the bay.

Following the technique of Lwiza *et al.* (1991), a least squares fit, with periods of 12.42 hours ($M_2$ tidal component) and 23.93 hours ($K_1$ tidal component), was applied to the time series of salinity, density, and velocity components at each gridpoint for which there was data from every transect repetition. The fit produced the amplitude and phase for each of the chosen periods and the subtidal signal. The combined diurnal and semidiurnal tidal signal was then reconstructed from these parameters. Although the fit used the periods of the $M_2$ and $K_1$

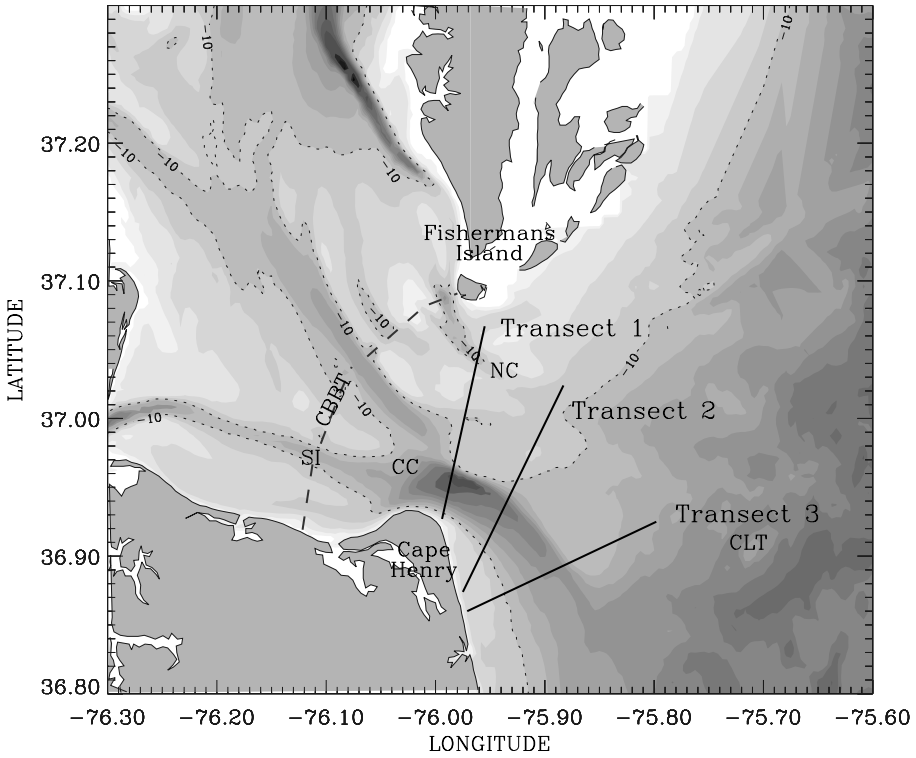


Figure 1. Lower Chesapeake Bay on the eastern coast of the United States. The map shows the locations of the three transects sampled during the cruise, with shaded bathymetry (dark tones are deep areas) and dotted lines marking the 10 m isobath. The Chesapeake Channel is marked as CC and the North Channel is marked as NC. The Chesapeake Bay Bridge-Tunnel (CBBT) is presented as a dashed line (marked as CBBT). The NOAA sea level and meterological station on the south island of the CBBT (marked as SI), and the NOAA meteorological station at the Chesapeake Light Tower (marked as CLT) provided wind and sea level information.

constituents, the 25-hr record from each transect was not sufficiently long to isolate these constituents from other semidiurnal ($N_2$ and $S_2$) and diurnal ($0_1$) constituents, so the fit actually reflected the combined effects of the semidiurnal constituents and the combined effects of the diurnal constituents. The least squares fit was effective in reproducing the observations along each of the transects, explaining a significant portion of the variability and yielding relatively low rms errors between fit and observed values (Figures 2, 3 and 4). The two component fit was better at Transect 1 than the other two transects, due to the reduced influence of tidal variability

at Transects 2 and 3. The fit for along-channel velocity was also generally better than that to across-channel velocity along each transect. An initial fit of the data to just the semidiurnal tidal component (not shown) generally explained 20-40% less of the variability and produced larger rms errors than did the fit with the two constituents. Similarly, adding an $M_4$ tidal constituent to the fit (not shown), did not produce noticeable improvement in either the amount of variability explained or in the rms error.

## DESCRIPTION OF OBSERVATIONS

### River discharge, water elevation and wind

The effects of river discharge at the bay mouth lag river discharge into the Chesapeake Bay by approximately one month, so the monthly averaged river discharge data from May were taken to be representative of the discharge conditions at the bay mouth in June. The monthly freshwater discharge data (Figure 5) indicated that high discharge conditions prevailed during the first six months of 1996 (which was a record year for freshwater discharge into the Chesapeake Bay), with values near 7,000 $m^3/s$ in January decreasing to near 4,000 $m^3/s$ from February through May, and continuing to decrease during the summer. May discharge amounts were relatively high, compared to the average monthly discharge of approximately 2,500 $m^3/s$ (Goodrich, 1988).

The beginning of the study period coincided with predicted spring tides for the month and the subsequent neap tide occurred on June 8, after the end of the study period. Comparison of the CBBT water elevation observations with predicted tidal elevations for the same station indicated that a sea-surface set-up of up to 0.35 m occurred at the bay entrance immediately before sampling on Transect 3 (Figure 6). This set-up was caused by a brief period of relatively strong (up to 10 m/s) onshore (easterly and northeasterly) winds on June 3. After that, the water elevation dropped abruptly on June 4 with the onset of moderate to strong northwesterly and then southwesterly winds. For the rest of the study period, the water elevations remained just slightly above predicted values (by 0.1 m), under weaker winds that shifted to a mostly easterly direction later in the day on June 5.

### Hydrography and Currents

Descriptions of the salinity and velocity data include intratidal features from the quasi-synoptic fields, and tidal properties and subtidal features from the fields reconstructed with the least squares fit.

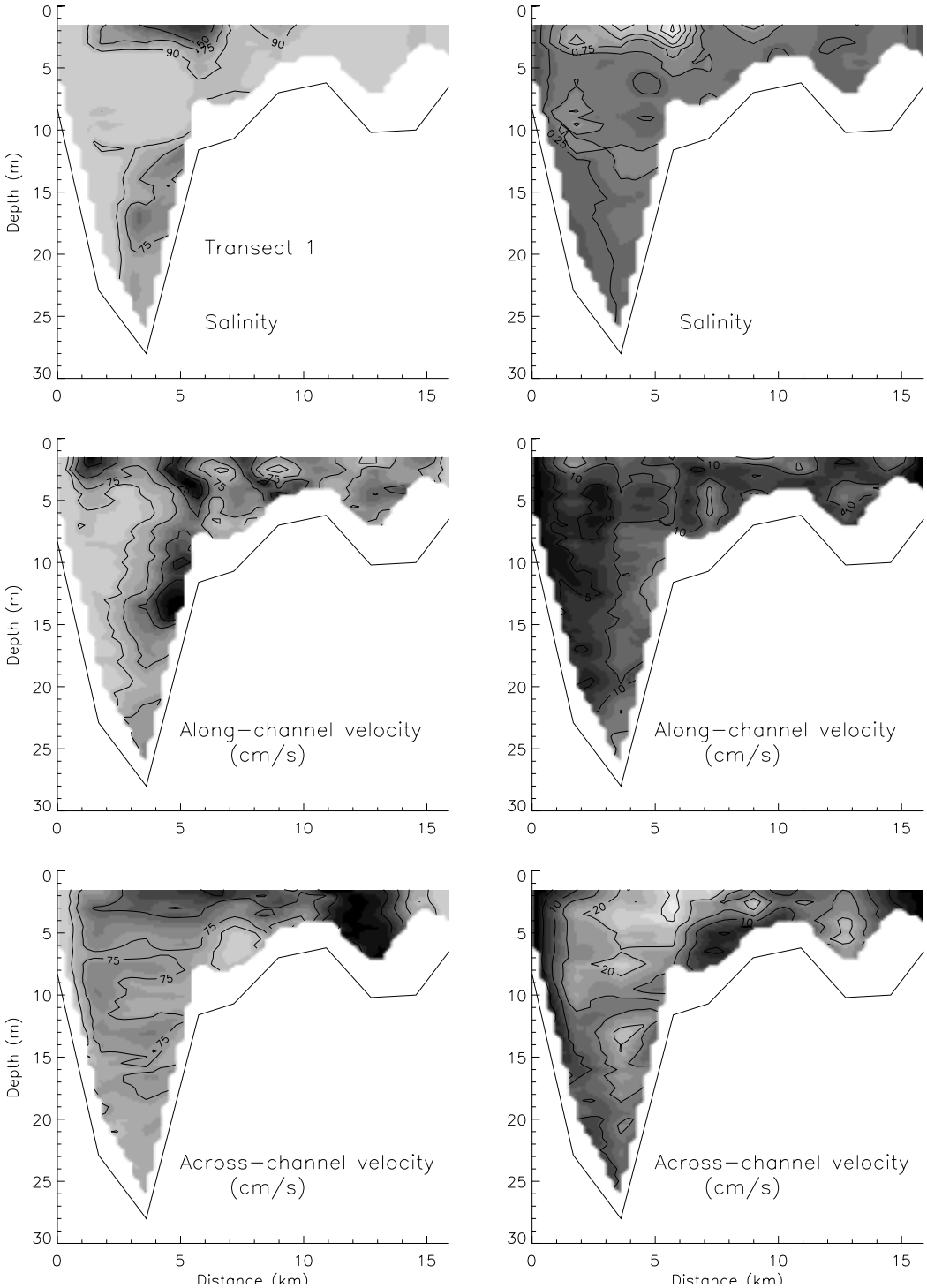


Figure 2. Percent variance explained by the least-squares fit to the semidiurnal and diurnal tidal frequencies (left column) and root-mean-square (rms) error between the fit and observed values (right column) for the salinity, along-channel velocity, and across-channel velocity fields of Transect 1. Percent variance is contoured at the 90, 75, 50 and 25 percent levels. Rms error contours are drawn at 0.25 psu intervals for salinity and 5 cm/s intervals for velocity. Lighter shading indicates higher values in each case and plots are drawn looking into the estuary.

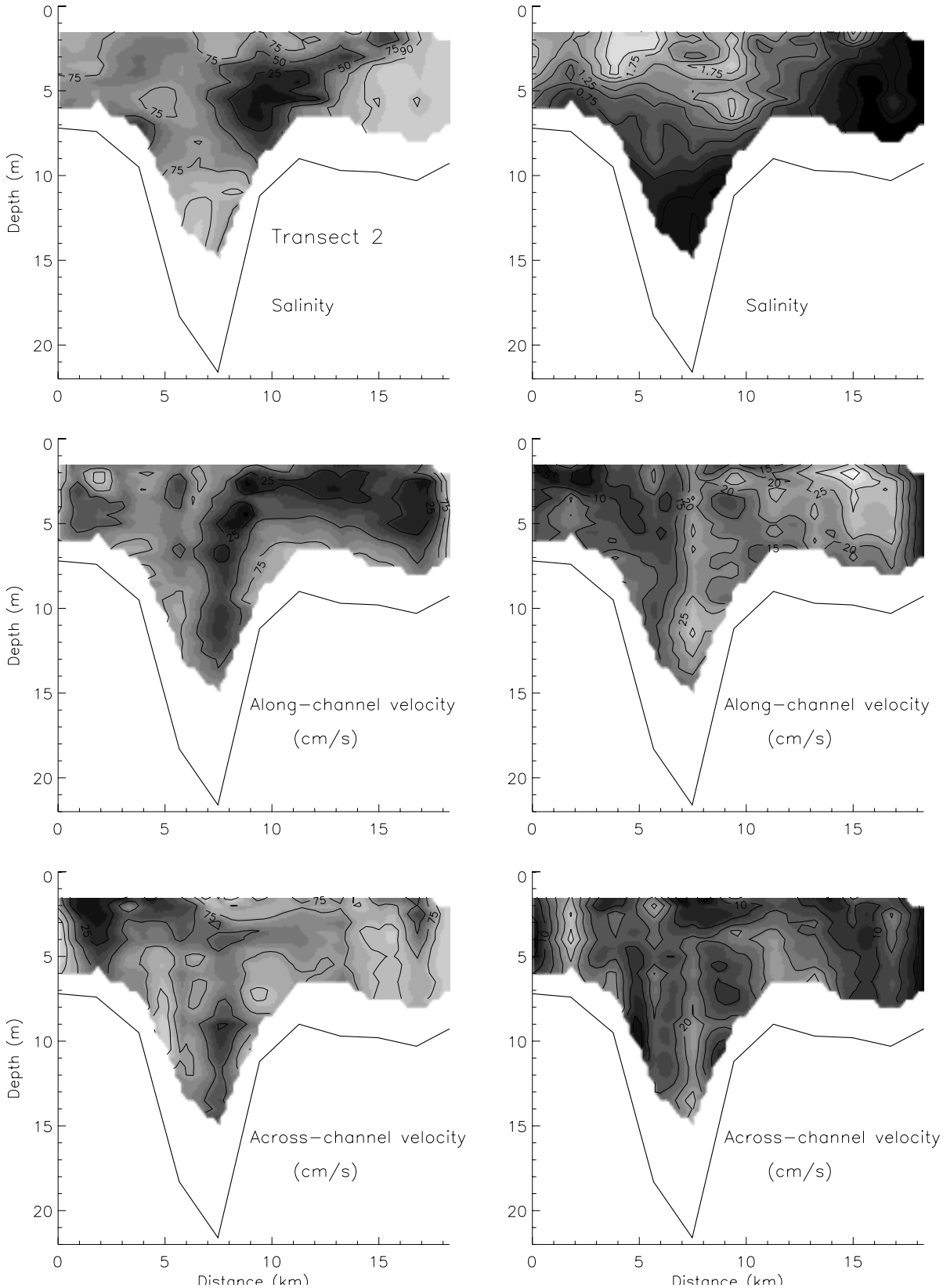


Figure 3. Same as Figure 2 for Transect 2.

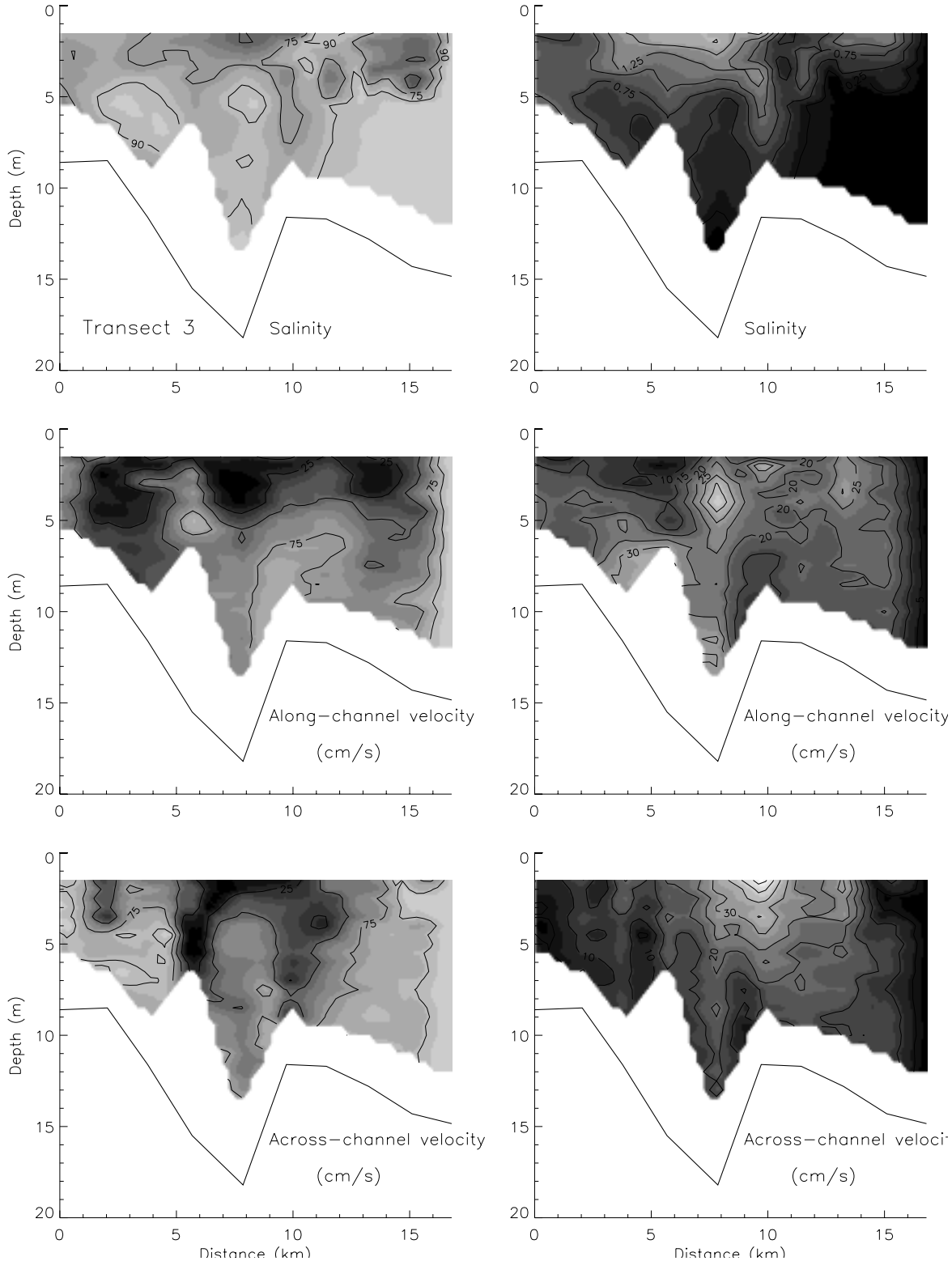


Figure 4. Same as Figure 2 for Transect 3.

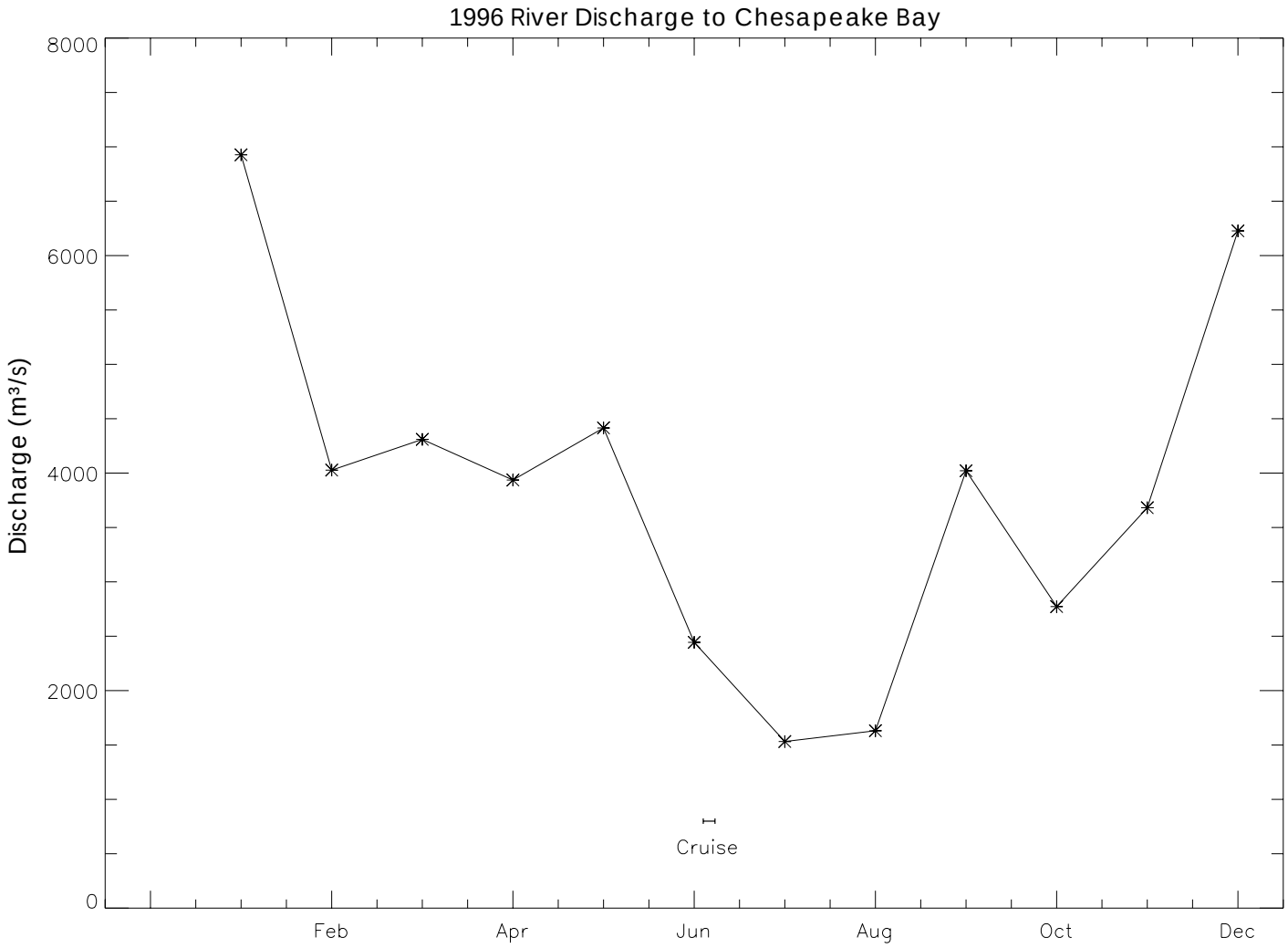


Figure 5. Monthly freshwater discharge ($m^3/s$) to the Chesapeake Bay for 1996, with the sampling period of this study marked on the plot. Note that freshwater forcing at the bay mouth lags river discharge by approximately one month.

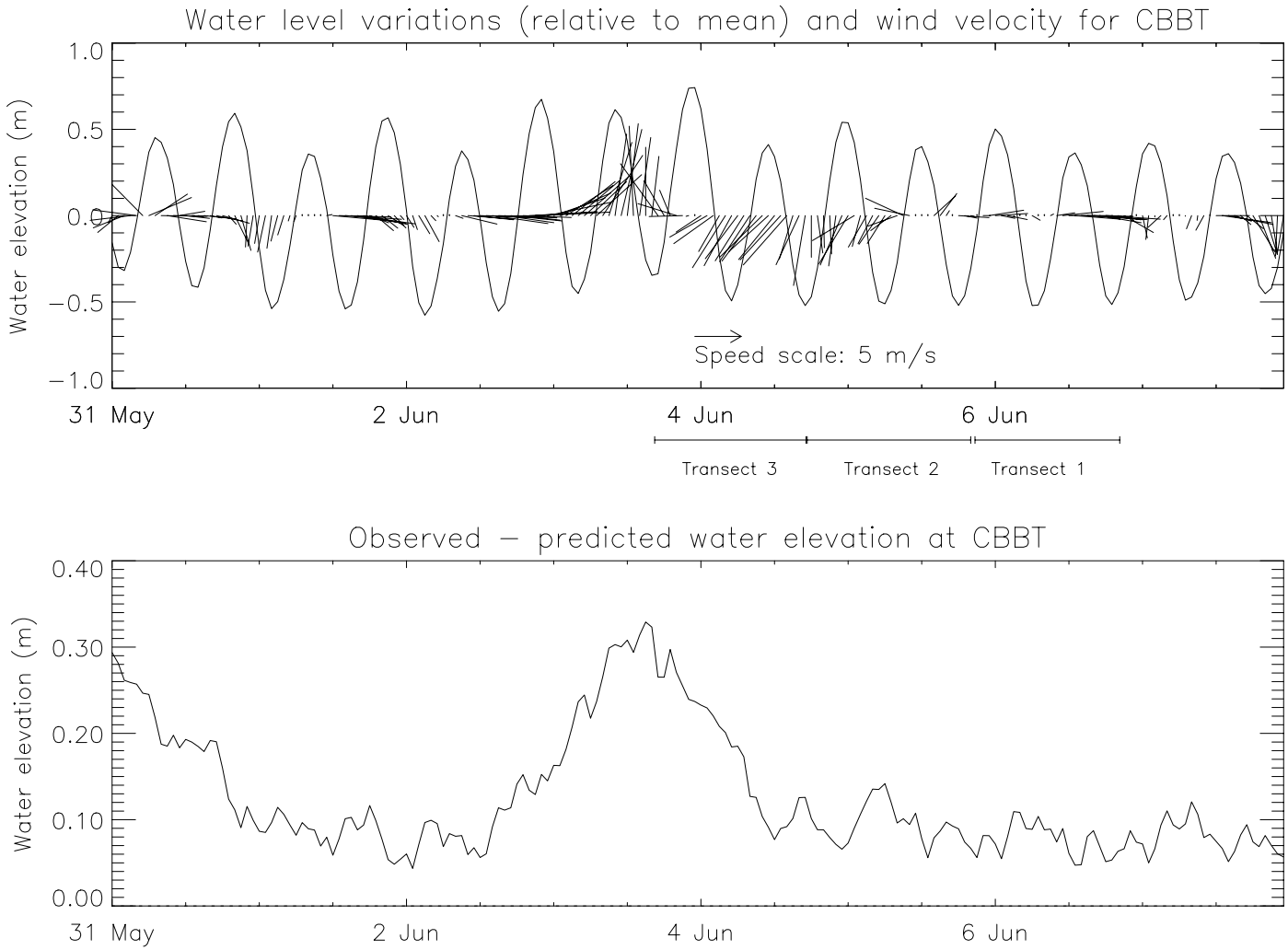


Figure 6. Water level variations, relative to sample mean, and wind velocity data from the NOAA tide gauge and meteorological station at the South Island of the CBBT (upper plot). Difference between observed and predicted water elevations at the CBBT tide gauge (lower plot). Wind direction is in the meteorological sense, indicating the direction that the wind is coming from. The duration of sampling along each transect is marked between the two plots.

**Intratidal Patterns**

Quasi-synoptic snapshots of salinity and velocity along each transect (Figures 7, 8 and 9) illustrate the intratidal salinity and flow variations during the study period. The substantial changes observed in the fields between successive transect repetitions illustrate the dynamic nature of the circulation in the plume region and the difficulty of capturing a truly synoptic picture. Features from the quasi-synoptic data fields are discussed below for each transect.

**Transect 1:** Along Transect 1 (Figure 7), stratification persisted throughout the tidal cycle in the channel, with fresher surface outflow over the more saline, subsurface inflow. The sharpest pycnocline developed just after maximum ebb tidal currents in the channel, with vertical density gradients as high as 4 $\sigma_t$ /m. Surface fronts developed over the northern shoulder of the channel near the time of maximum flood currents in the channel and were associated with horizontal surface convergence in the across-channel velocities (repetition 8). Near the end of flood currents, a narrow band of higher salinity water intruded along the southern coast, creating a second surface front between these shelf waters and the buoyant surface outflow that was pushed slightly offshore. Over the shoals in the northern portion of the transect, the water column was vertically mixed for most of the sampling period, with salinity increasing to the north.

The strongest instantaneous along-channel currents (0.8 m/s) of Transect 1 occurred as inflow over the channel, within a subsurface core centered at approximately 15 m depth (repetition 8). Outflow velocities reached 0.7 m/s at maximum ebb, generally with maximum currents at the surface, although subsurface maxima were also found over the shoals. Vertical shears in the along-channel flow were as high as 0.2 $s^{-1}$ over the channel when ebbing surface currents opposed flooding currents at depth (repetition 1). The instantaneous across-channel velocities were generally smaller than the along-channel velocities, but did reach up to 0.7 m/s (repetition 5). Examination of vector plots (not shown) indicated that these high across-channel velocity values occurred as tidal currents rotated from outflow to inflow after the end of ebb currents.

**Transect 2:** The channel of Transect 2 was located further offshore than it was on Transect 1, but the most stratified conditions (up to 4 $\sigma_t$ /m) still occurred over the channel just after maximum ebb currents (Figure 8). Surface fronts developed over the north shoulder of the channel (repetitions 6 and 8), and at times over the south shoulder as well (repetition 6), as was observed by Sanders and Garvine (1996) for the Delaware Coastal Current. The sharpest front occurred towards the end of flood currents over the northern shoulder of the channel (repetition 6), however, a front also occurred over the same shoulder shortly after maximum surface ebb currents in the channel (repetition 8). The buoyant plume moved laterally to a much greater extent than it did in Transect 1, with the core of lower salinity surface water moving completely across the transect during the tidal cycle.

Instantaneous velocity fields over Transect 2 had highest values (1.3 m/s) in a northwestward (inflow) subsurface jet in the channel associated with the flood tide. The strongest southeastward flow (outflow) reached 0.9 m/s, with surface maxima found both over the channel and over the shoals. Relatively strong subsurface outflow was also found over the shoals and southwest channel shoulder, similar to the Transect 1 data. Vertical shears in the along-channel local instability in the density fields evident at the location of the highest velocity shears

(repetition 1). In contrast to Transect 1, high vertical shear in the along-channel velocity was also found over the northeastern shoal, rather than being confined to the channel. This high shear accompanied the lateral movement of the plume over the shoal. The instantaneous across-channel flow of up to 0.6 $s^{-1}$ and development of a sharp pycnocline occurred after maximum ebb currents, with low was also significant, reaching up to 0.7 m/s when tidal currents rotated between ebb and flood stages. Surface front formation was again associated with horizontal convergence in the across-channel flow (repetition 3).

**Transect 3:** Enhanced stratification over the channel, with more homogeneous conditions over the shoals was also found along Transect 3 (Figure 9). As in the previous transects, the pycnocline sharpened (vertical density gradients up to 2 $\sigma_t$ /m) over the channel as saline inflow at depth opposed the ebbing surface flow (repetition 1). A surface front (6 $\sigma_t$ in 1300 m horizontal distance) appeared over the right (looking into the bay) shoulder of the channel at the end of flood currents in the channel (repetition 4). The low salinity plume extended across most of the transect at times, with surface flood currents over the channel occasionally separating two surface salinity minima over the shoals on either side (repetitions 6 and 7).

The instantaneous velocity fields of Transect 3 exhibited a subsurface inflow jet (1.3 m/s) during flood, and a slightly weaker (0.7 m/s) surface outflow maximum during ebb. Over the channel and eastern shoal, vertical shears in the along-channel flow of up to 0.2 $s^{-1}$ were again found when surface ebb flow opposed flood currents at depth (repetition 1). In the channel, flow was persistently northwestward (toward the bay mouth), and even the surface currents did not always reverse direction toward the southeast during ebb, but simply decreased in magnitude. The across-channel flow had maximum values reaching 1.1 m/s. Strong horizontal convergence of the across-channel flow was again associated with the formation of surface fronts (repetitions 1 and 4).

### Tidal Patterns

Along Transect 1, a maximum in the semidiurnal tidal amplitude of the salinity field, extended north from the southern side of the transect, centered at 4 to 6 meters depth (Figure 10). This maximum was due to the relatively large salinity variations associated with the lateral movement of the surface plume and intrusion of more saline shelf water along the southern coast. Both the semidiurnal and diurnal amplitudes in salinity were reduced at depth in the deep channel, as bottom friction reduced the tidal excursions. The semidiurnal tidal amplitude of the along-channel velocity had a subsurface maximum centered over the deep channel, decreased over the shoals, and then increased slightly over the North Channel. The semidiurnal phase of the along-channel velocity also varied laterally, with the shoals and the southern side of the channel leading the center portion of the deep channel. The diurnal along-channel velocity amplitudes had a subsurface maximum over the south side of the channel, a minimum near the surface over the northern shoulder of the channel, and a secondary surface maximum over the shoal area. The across-channel velocity had semidiurnal and diurnal tidal amplitude maxima over the channel.

Similar features were found in the tidal properties along Transect 2 (Figure 11) and Transect 3 (Figure 12), with highest amplitudes tending to occur in the channel and phase leading near the bottom relative to the surface and over the shoals relative to the channel. In some cases, amplitude maxima occurred below the surface, near the pycnocline. The amount of spatial

variability in the amplitude and phase contours probably reflected difficulty in resolving the intratidal flow reversals with the given station spacing in distance and time between stations.

**Subtidal Patterns**

**Transect 1:** The subtidal salinity and velocity fields for Transect 1 are shown in Figure 13a. Lowest salinity water was confined to a core, approximately 3 km wide, at the surface over the southern side of the Chesapeake Channel, separated from Cape Henry. Highest salinity water along the transect was found in the deepest part of the Chesapeake Channel. At the surface there was along-channel outflow over the north shoulder of the deep channel associated with the plume (0.3 m/s maximum), a narrow inflow along the coast off Cape Henry and an inflow maximum (0.25 m/s) over the shoal. A weak outflow (northeastward) was present at all depths in the North Channel. Along the southern coast, the plume narrowed with increasing depth, reaching a depth of 10 m. In the deep channel, the outflowing surface vectors rotated anticyclonically with depth to an inflow (northwestward) direction. The transition to inflow occured at shallower depths over the channel axis and at greater depths over the shoals. The deeper flow was into the bay, aligned with the Chesapeake Channel and reaching a subsurface maximum of 0.4 m/s. The across-channel subtidal velocities were smaller than the along-channel velocities, with maximum values of 0.2 m/s and most values less than 0.1 m/s. Subtidal surface convergences of order $10^{-4}$ $s^{-1}$ were found over each side of the Chesapeake Channel, with surface divergences of similar magnitude over the center of the deep channel and over the shoal.

**Transect 2:** The subtidal, low salinity surface plume was also centered over the channel along Transect 2 (Figure 13b), with higher values than those observed on Transect 1, as expected, since Transect 2 was further from the bay mouth. Surface salinities increased over the shoal areas on each side, with higher surface values on the seaward side and highest overall salinity found in the bottom of the channel. The along-channel velocity had a surface outflow (southeastward) maximum over the seaward shoulder of the channel (0.25 m/s) with outflow continuing over the seaward shoal, but surface inflow present along the coast. At greater depths, the flow near the coast continued to flow toward the bay mouth, while flow along the rest of the transect rotated anticylonically with depth from outflow to inflow. Below approximately 8 m depth, all flow was towards the bay mouth and aligned with the bathymetry, with a subsurface maximum (0.6 m/s) in the center of the channel. The across-channel subtidal flow was again weaker than the along-channel flow (maximum near 0.25 m/s) and had horizontal convergences of up to $10^{-4}$ $s^{-1}$ over both shoulders of the channel.

**Transect 3:** The subtidal, low salinity plume was quite broad along Transect 3, but was still centered over the channel (Figure 13c). Highest salinities were now found at depth at the offshore end of the transect, rather than in the channel, because the channel was not much deeper than the offshore station. The subtidal outflow (southeastward) was weak (< 0.1 m/s) and was only found above 2 meters depth, seaward of the center of the channel, with weak inflow at the surface on the landward half of the transect. The subtidal flow reflected the influence of offshore plume movement as winds shifted to a southerly direction during sampling on this transect. The surface outflow rotated quickly to inflow (northwestward) with increasing depth, and only inflow was found below 4 m depth. The vertical rotation was again anticyclonic, and occurred at shallower depths in the channel and deeper depths over the shoals. With increasing depth, the

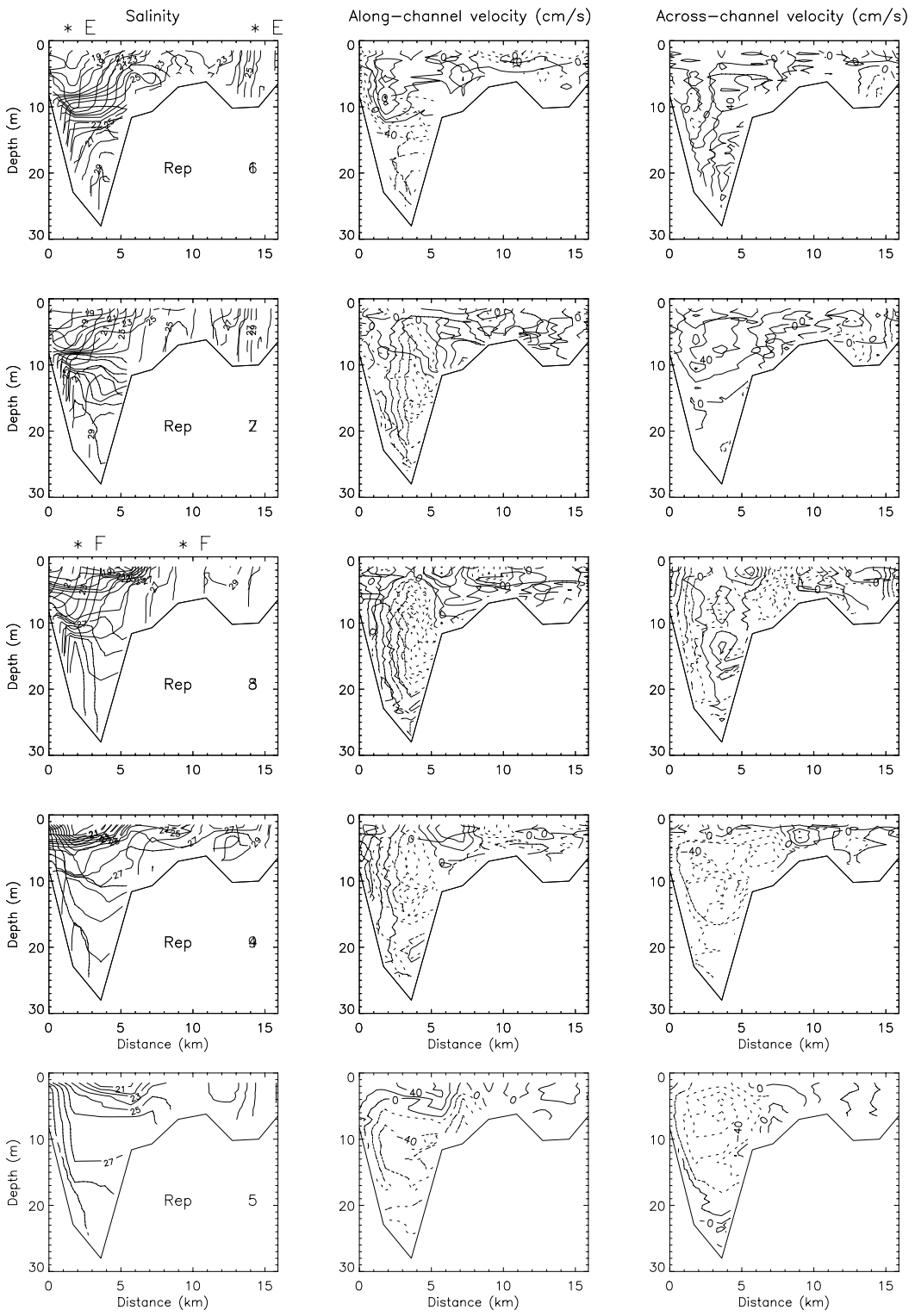


Figure 7. Contoured salinity, along-channel velocity and across-channel velocity data for successive repetitions of Transect 1. Contours are drawn at intervals of 1 salinity unit and 5 cm/s for velocity. Positive values of along-channel velocity indicate flow out of the bay, and positive values of across-channel velocity indicate northward flow. Times of maximum flood and ebb currents at depth in the channel are marked with asterisks above the salinity plot. Plots are drawn looking into the estuary.

# TRANSECT 1

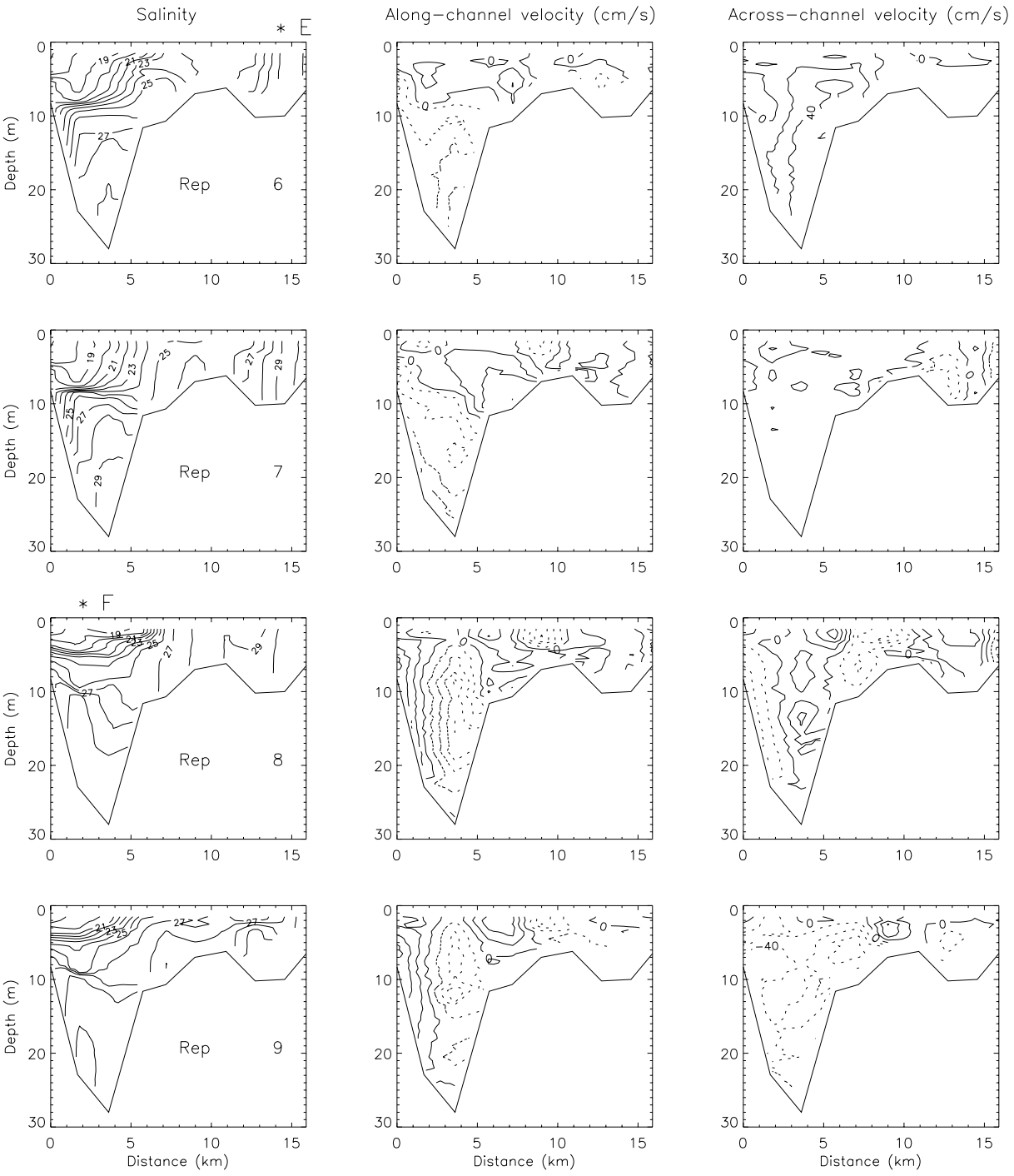
Salinity
Along−channel velocity (cm/s)
Across−channel velocity (cm/s)
* E
* F
Depth (m)
Rep 6
Rep 7
Rep 8
Rep 9
Distance (km)

# TRANSECT 2

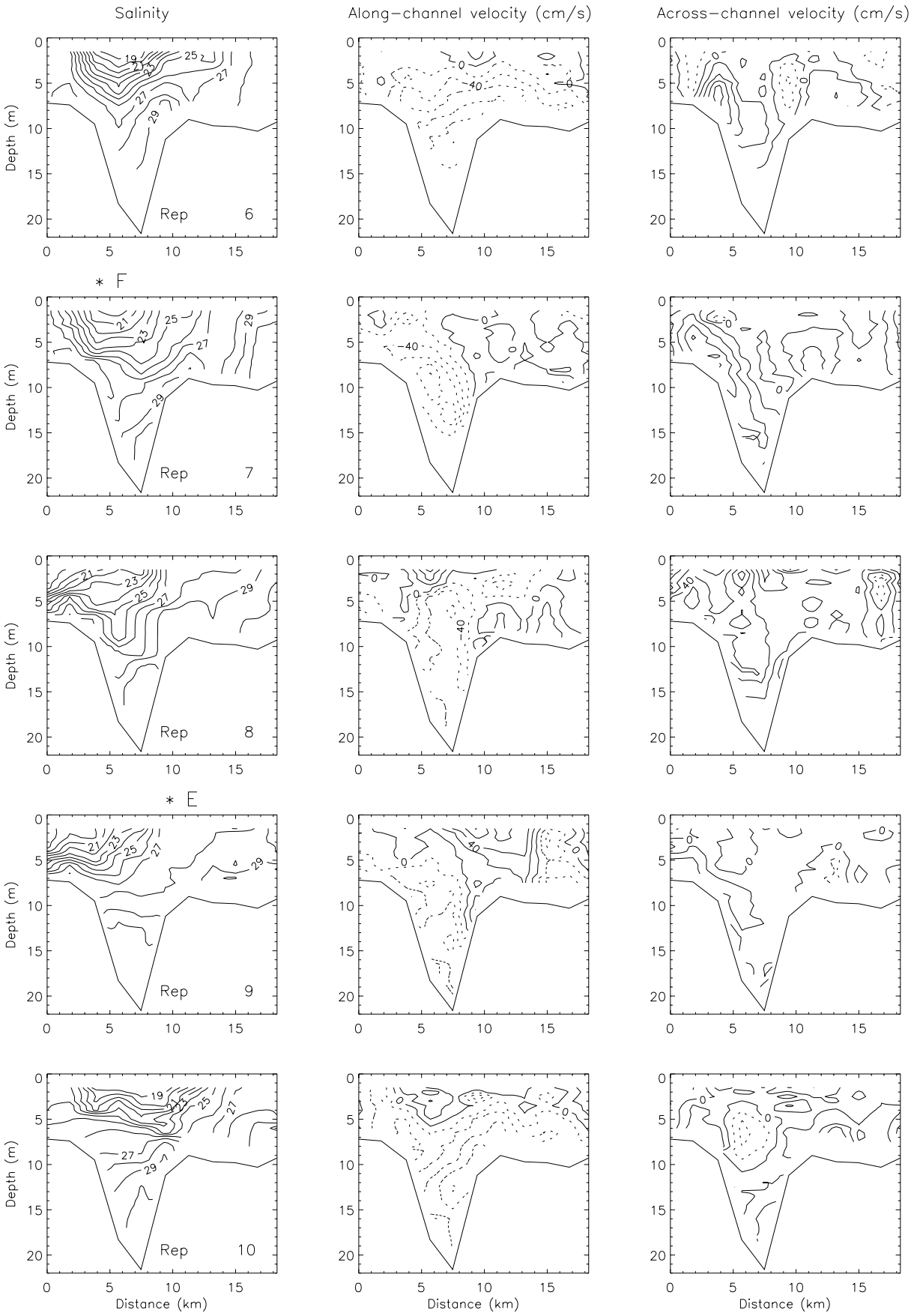
Salinity
Along−channel velocity (cm/s)
Across−channel velocity (cm/s)
Depth (m)
Rep 6
* F
Rep 7
Rep 8
* E
Rep 9
Rep 10
Distance (km)

# TRANSECT 2

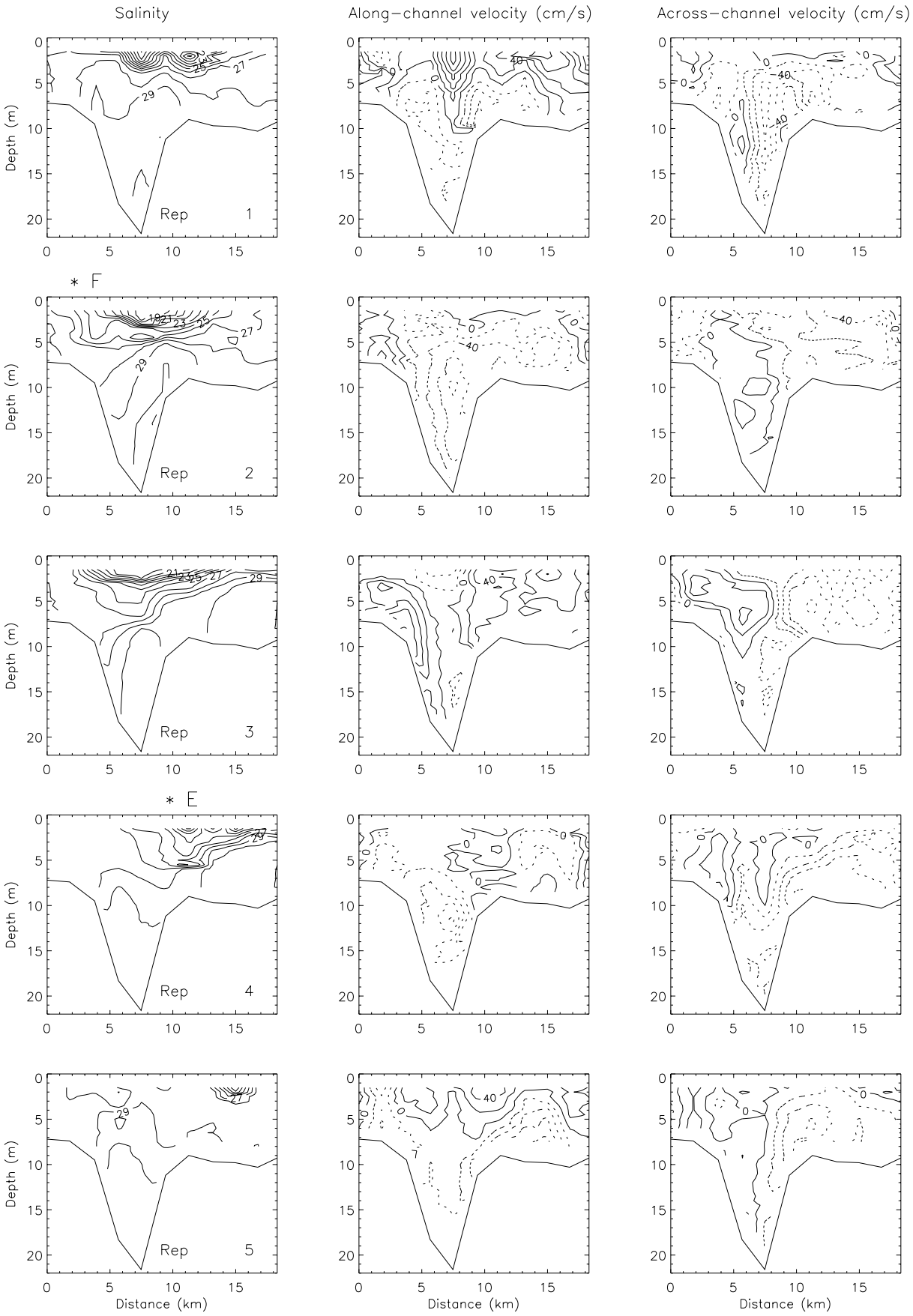
Salinity
Along−channel velocity (cm/s)
Across−channel velocity (cm/s)
Depth (m)
Rep 1
* F
Rep 2
Rep 3
* E
Rep 4
Rep 5
Distance (km)

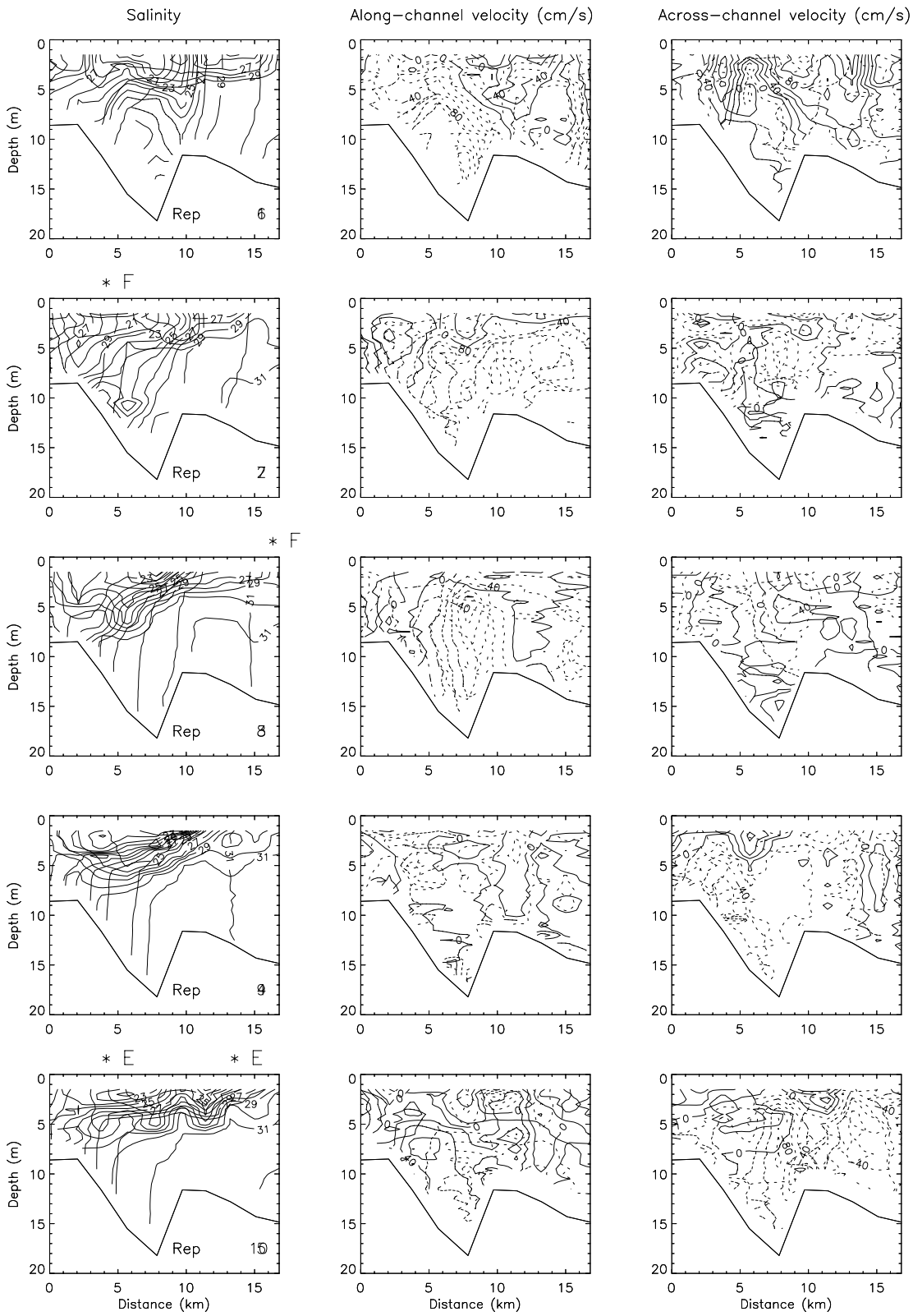


Figure 9. Same as Figure 7 for Transect 3. Positive values of along-channel velocity indicate northwestward flow toward the bay mouth. Positive values of across-channel velocity indicate east-northeastward or seaward flow.

# TRANSECT 3

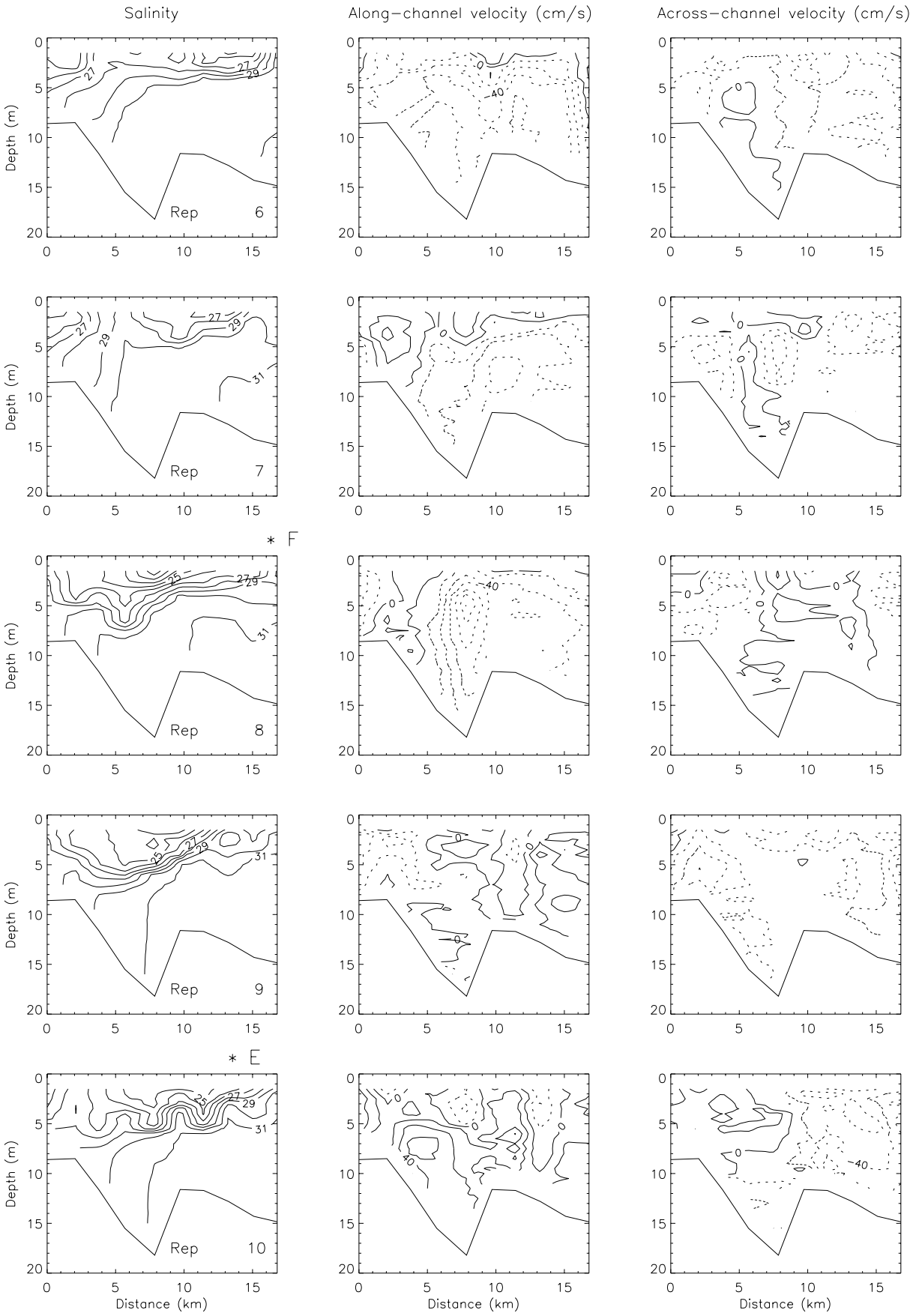
Salinity
Along−channel velocity (cm/s)
Across−channel velocity (cm/s)
Depth (m)
Rep 6
Rep 7
* F
Rep 8
Rep 9
* E
Rep 10
Distance (km)

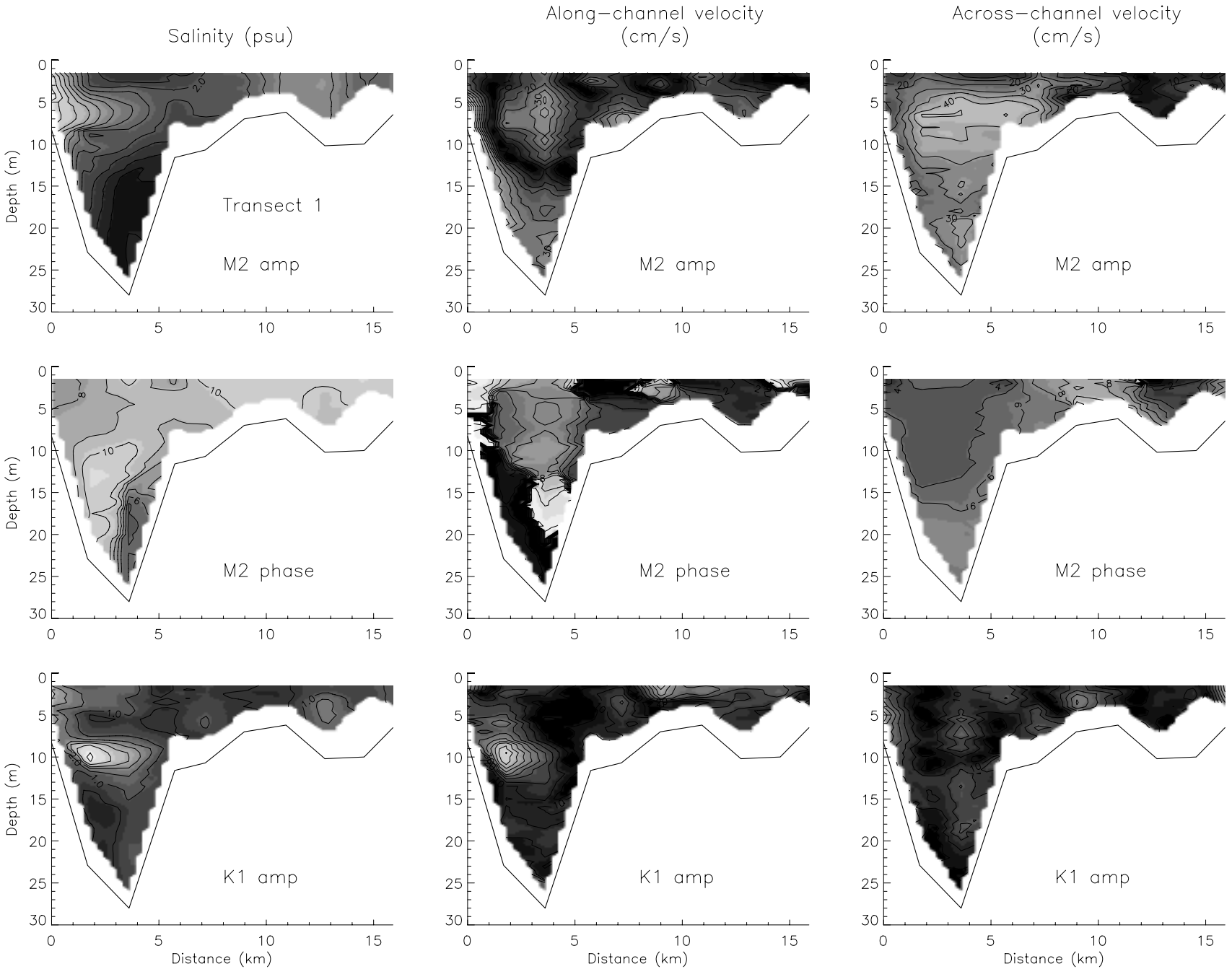


Figure 10. Contoured semidiurnal amplitudes and phases and diurnal amplitudes for salinity, along-channel velocity and across-channel velocity for Transect 1. Tidal amplitudes are contoured at intervals of 0.5 salinity units and 5 cm/s for velocity. Tidal phases are contoured at 1 hour intervals. Lighter shading indicates higher values in all cases and plots are drawn looking into the estuary.

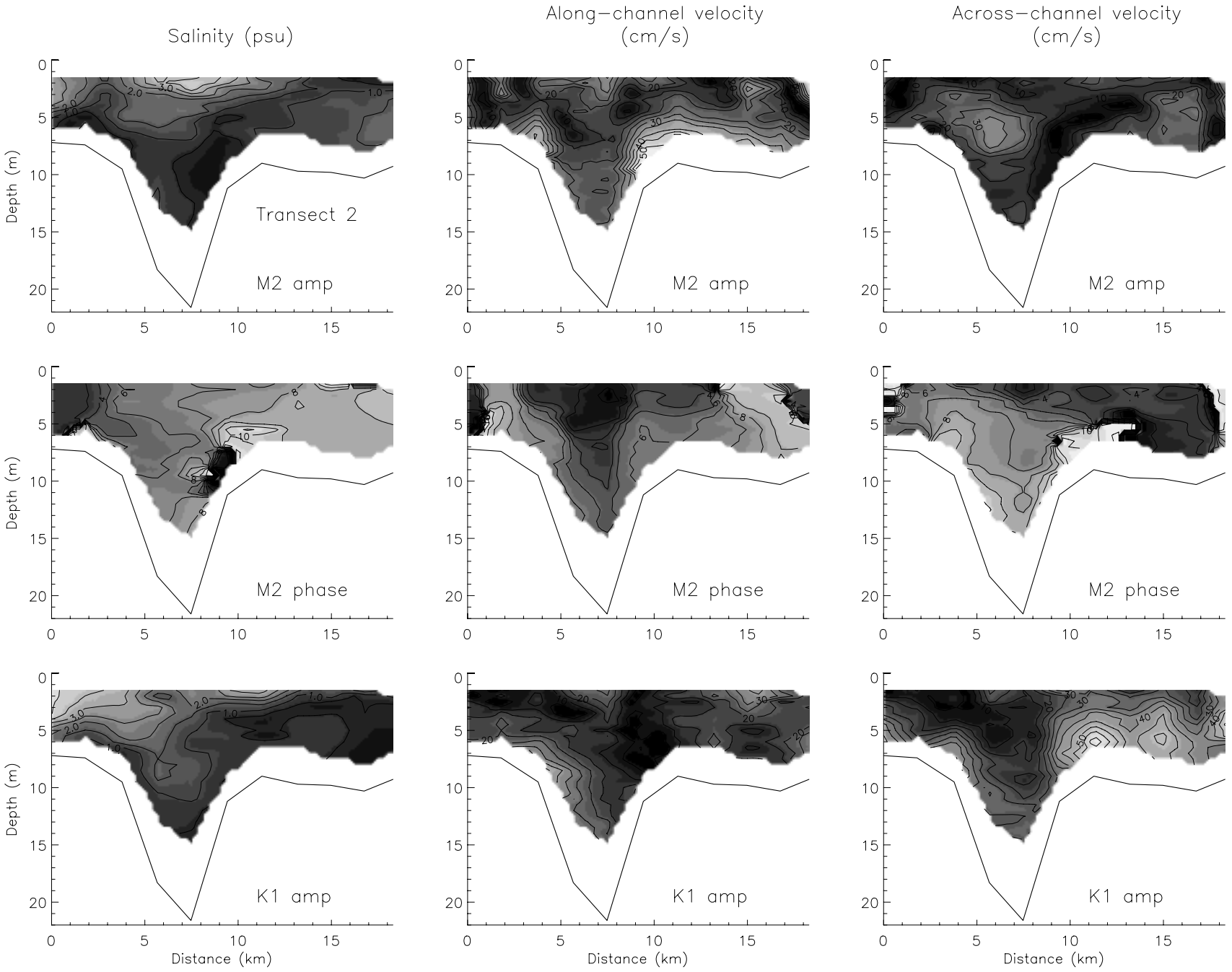


Figure 11. Same as Figure 10 for Transect 2.

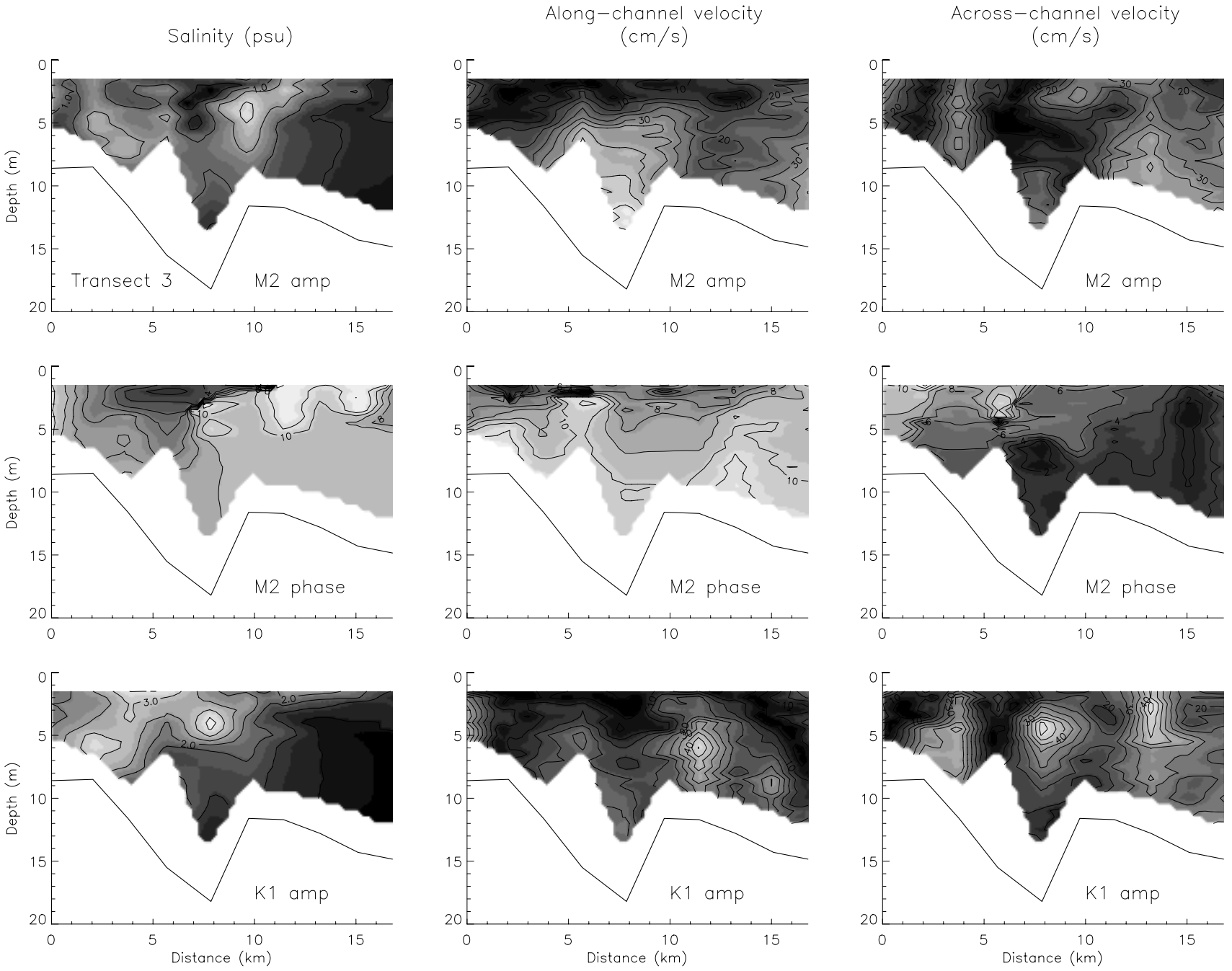


Figure 12. Same as Figure 10 for Transect 3.

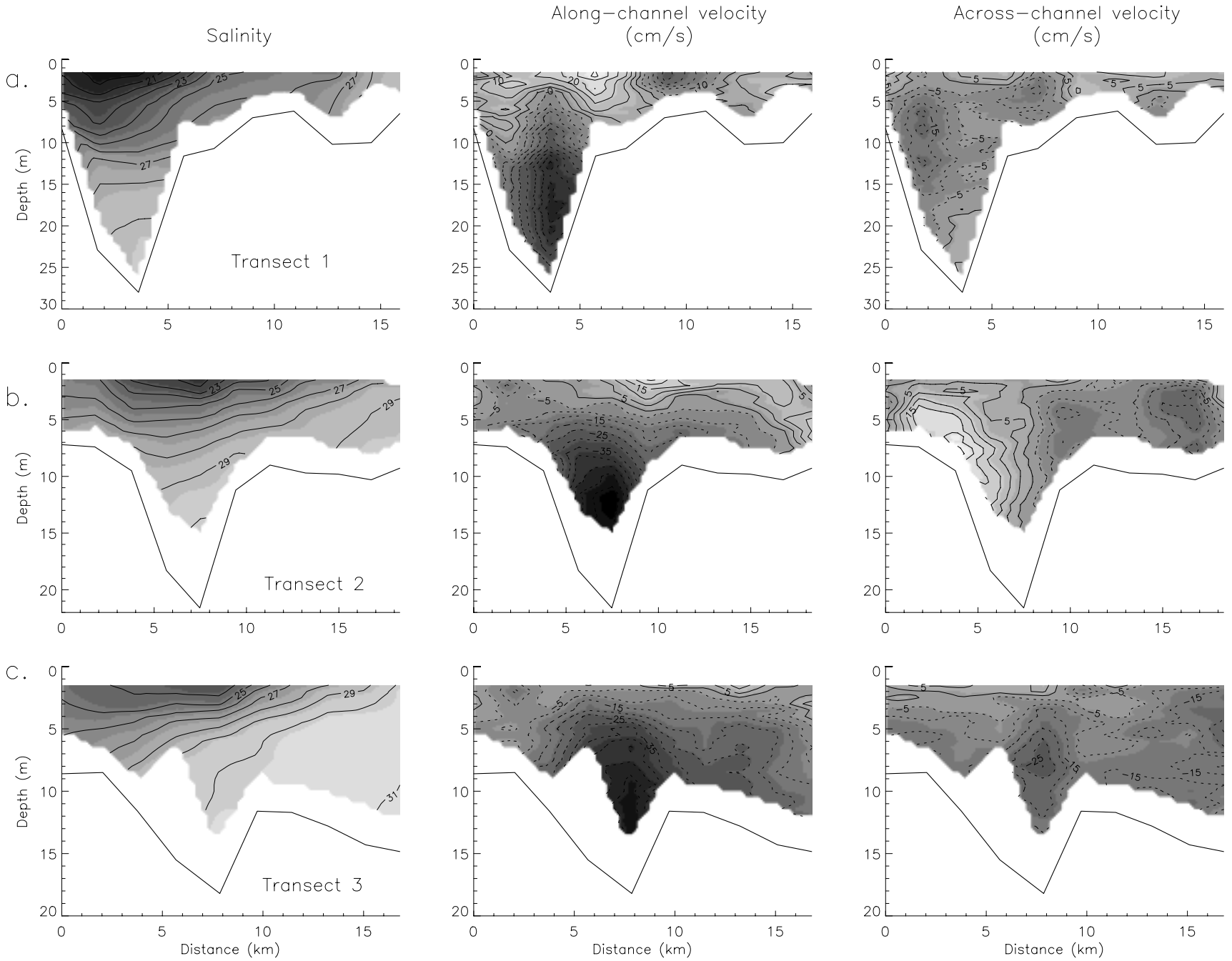


Figure 13. Contoured subtidal salinity, along-channel velocity and across-channel velocity data for: a. Transect 1, b. Transect 2, and c. Transect 3. Salinity data are contoured at intervals of 1 salinity unit and velocity data are contoured at 5 cm/s intervals. Plots are drawn looking into the estuary.

inflow aligned with the channel bathymetry, reaching a subsurface maximum of 0.5 m/s in the channel. The across-channel velocity was mostly landward, with a subsurface maximum (0.3 m/s) in the channel. Seaward across-channel velocities were found near the surface on the southern side of the transect, producing horizontal surface convergences of order $10^{-4}$ $s^{-1}$ over the seaward shoulder of the channel.

## DISCUSSION

Earlier studies in the region of the Chesapeake Bay entrance (Boicourt, 1981; Goodrich, 1987; Valle-Levinson and Lwiza, 1995; Valle-Levinson and Lwiza, submitted) have described mean flow patterns and looked at features such as the influence of the channel/shoal bathymetry on lateral locations of the flow. Numerical simulations of estuary-shelf circulation patterns induced by wind, tidal and gravitational forcing have shown that these mean flows may affect larval recruitment through the transport and dispersal of planktonic larvae to and from the Chesapeake Bay (Johnson and Hess, 1990). Smaller-scale circulation features will also impact processes such as larval recruitment if their time and space scales match the scales associated with the biological processes, such as spawning location and duration of the larval stage. Therefore, characterizing and understanding the smaller-scale patterns in the hydrographic and flow fields at the bay mouth, under various forcing conditions, is a necessary part of understanding the variability in processes such as larval recruitment. In this study, we used hydrographic and velocity observations, collected at a 2 km spatial resolution, to examine such smaller-scale features in the intratidal, tidal and subtidal fields at the bay mouth and in the offshore plume region. Our study period was characterized by high freshwater discharge and moderate wind forcing conditions. Tidal forcing was also relatively strong, with spring tides occurring at the beginning of the cruise.

**Intratidal patterns:** High spatial and temporal variability in the intratidal salinity and flow fields were observed in this study along all three transects (Figures 7, 8 and 9). Stratified conditions and two-way flow persisted over the Chesapeake Channel on all three transects (also occurring to a lesser extent in the North Channel along Transect 1), while vertically homogeneous conditions and unidirectional currents predominated over the shoals for most of the tidal cycle. Depth-independent tidal flow over the shoals was associated with increased vertical mixing (either tidally-induced or wind-driven) in shallow waters, while higher stratification and two-way circulation in the channel indicated the greater influence of gravitational forcing. In the channels, maximum vertical stratification occurred towards the end of ebb currents due to tidal straining (Simpson, *et al*, 1990), as has also been observed by Valle-Levinson and Lwiza (1995) along a transect upstream of the CBBT. Strong vertical shears of up to 0.4 $s^{-1}$ in the along-channel velocity and sharp pycnoclines (with vertical density gradients of up to 4 $\sigma_t$ /m) developed in the channel along each transect when surface outflow opposed subsurface inflow. Bulk Richardson numbers were calculated for local areas of high velocity shear in the water column and ranged from 0.03 to 1.0, with values less than 0.25 indicating that shear instability may sometimes dominate the density distribution at vertical scales of ~l m. Vertical spreading of the isopycnals was observed in some cases in these regions, and the observation of stronger velocity shears (0.6 $s^{-1}$) along Transect 2 was accompanied by indications of instability in the density data over ~1 m depth. However, the density contrast between the fresher surface outflow and more saline inflow maintained stratification over the entire water column in each case.

Surface fronts developed over the right shoulder of the channel (looking into the estuary) along all three transects, and were associated with horizontal convergence in the across-channel velocity. These fronts developed at different stages of the tidal flow in the channel, including after maximum ebb currents (Transect 2, repetition 6), near maximum flood currents (Transect 1, repetition 8), and near the end of flood currents (Transect 2, repetition 8; Transect 3, repetition 4). The front that formed in the latter stages of ebb flow along Transect 2 was accompanied by a second front over the left shoulder of the channel, suggesting formation of a plume front along the edge of the advancing plume, which was centered over the channel at that time. Frontal formation at the other stages of the tide appeared to be associated with large phase shifts (up to 3 hrs) between tidal flow over the shoals and in the channel, which produced horizontal velocity convergence over the right shoulder of the channel. Along Transect 1, formation of a front offshore from Cape Henry was associated with the inflow of shelf water and surfacing of isohalines along the coast near the end of flood currents.

Increased lateral movement of the low-salinity core of the plume towards and away from the coast in the offshore region south of Cape Henry (Figures 8 and 9), relative to the bay mouth (Figure 7), was associated with the increased influence of inertial effects as the plume exited the bay and with temporal changes in wind forcing. Away from the mouth, inertial effects were expected to be most influential at maximum ebb currents, when the surface velocities were strong enough to overcome the tendency of the Coriolis force to constrain the plume to the coast. There was some evidence of this behavior along Transect 2 (repetition 4), but, overall, wind forcing appeared to have more of an effect than inertial forcing on lateral plume location along both Transects 2 and 3. At the beginning of sampling on Transect 3, relatively strong (near 10 m/s) northerly and northwesterly winds prevailed, then shifted to southwesterly (Figure 6). The salinity minimum and strongest southward surface flow were located close to the coast at the beginning of the sampling period (Figure 9, repetitions 1-3) and then migrated offshore after the onset of southwesterly winds (Figure 9, repetition 4). So offshore movement of the plume along Transect 3 was associated with direct frictional coupling of the southwesterly winds with the ocean surface and subsequent offshore transport. Along Transect 2, the salinity minimum associated with the plume remained offshore (Figure 8) until after the winds shifted from a southerly (with speeds of 5-10 m/s) to more northerly direction (5 m/s). As the southwesterly winds relaxed and then shifted to a northerly direction, the plume moved toward the coast and remained there through the remainder of sampling along Transect 2, suggesting that northerly winds (or the absence of southwesterly winds) allowed the plume to return to the coast. Thus, the instantaneous lateral location of the offshore surface plume did appear to be strongly influenced by wind forcing. At Transect 1, the low-salinity plume remained relatively close to the coast during the entire period (Figure 7), under light, easterly wind conditions.

**Tidal patterns:** The semidiurnal tidal constituent was consistently more important than the diurnal constituent for salinity and along-channel velocity, but the diurnal constituent was still significant and necessary to produce a fit that reproduced the observations reasonably well. The two-constituent fits to the salinity and along-channel velocity data were better along Transect 1 than either of the other two transects, with smaller rms differences between the observed and fit values and a greater amount of variance explained. The better performance of the fit along Transect 1 indicated that tidal forcing was relatively more important at the bay mouth than in the region immediately offshore from the mouth (or conversely, that the offshore region was affected

more by nontidal processes), which is consistent with the previously discussed links between wind forcing and the observed intratidal patterns. Some tidal amplitude maxima were located near the surface over the channel, as had been found by Valle-Levinson and Lwiza (1995) further inside the bay. However, in some cases the tidal amplitude maxima in the channel also occurred below the surface, near the mean pycnocline. As discussed by Jay and Smith (1990) for data from the Columbia River, stratification can inhibit vertical turbulent momentum transfer and enhance shear in the water column. Numerical simulations by Haskell *et al.* (submitted) indicate that this inhibition of vertical momentum transfer in the pycnocline may dampen upward transmission of the tidal phase, resulting in a subsurface maximum tidal amplitude under high stratification. Tidal amplitude maxima were also found over the channel shoulders or shoals, but some of this structure may simply have reflected the difficulty of capturing a highly variable flow field with data from stations at intervals of approximately 2 km in distance and up to three hours in time. Tidal phase shifts of up to 3 hours were observed between the channel and shoals and from surface to bottom in the channel. These phase shifts appeared to be important in producing horizontal velocity convergence over the right (looking into the bay) shoulder of the channel.

**Subtidal patterns:** The greatest subtidal flow of shelf water directed towards the bay was found in the channel on all three transects, despite differences in the lateral location of the channel along the transect. So, the effects of bathymetry appeared to outweigh the effects of Coriolis, which would tend to confine the inflow to the right side of the transect (looking into the bay). These findings are consistent with the results from Boicourt (1981) and Goodrich (1987) for moored current meters in the region, from the ADCP measurements by Valle-Levinson and Lwiza (1995), and with the numerical results of Valle-Levinson and O'Donnell (1996). Similarly, the location of the subtidal outflow plume was not constrained to the left side of each transect, but was separated from the coast, with the salinity minimum located over the channel axis and higher surface salinity found to the left of the channel. This persistent, two-way subtidal exchange in the channel, with outflow at the surface and inflow at depth, reflected the influence of gravitational forcing on flow in the channel.

The influence of wind-forcing was also evident in the subtidal velocity fields along Transect 3, as the predominantly northward flow across the transect reflected the prevailing southerly winds (Figure 13c). The light to moderate (5 m/s) east-southeasterly and easterly winds that prevailed during the transits of Transect 1 may have driven the subtidal inflow observed over the shoal (Figure 13a), since the winds would have the most impact on circulation in that shallow (approximately 6 meter depth) area. The tidal fits for both salinity and along-channel velocity explained relatively less of the data variability over this shoal, another indication that subtidal forces were important. However, subtidal surface inflow over this shoal has been frequently observed, under all but southwesterly wind conditions, as part of an anticyclonic gyre formed between this inflow and outflow over North Channel (Valle-Levinson, *et al*, submitted). The inflow over the shoal has been attributed to the effects of tidal rectification over a channel-shoal bathymetry, as discussed by Li and O'Donnell (1997). Since stratification was reduced or absent over this shoal area, wind-forcing and tidal rectification would be expected to dominate over gravitational forcing, thus producing the observed inflow.

The separation of the subtidal plume from the coast along all three transects and persistent near-surface inflow along Cape Henry were consistent with development of an anticylonic gyre in

the subtidal velocity field as the plume left the bay mouth. Such gyres have been observed by Geyer and Signell (1990) around a headland in Vineyard Sound, Massachusetts, modeled by Klinger (1994) around a rounded cape, and generated in numerical simulations of circulation at the Chesapeake Bay mouth (Valle-Levinson *et al.*, 1996). Our observations are consistent with Klinger's (1994) hypothesis that upwelling of the pycnocline can control separation of a density current from a rounded cape, when the coastline's radius of curvature is small enough that centrifugal forces become significant. The Rossby number ($R_o = u/fL$) is close to unity for the observed subtidal plume width and velocity along Transect 1 ($R_o$=1.1 for $u$=0.3 m/s and $L$=3 km). Therefore, the formation of this gyre may be sensitive to changes in forcing, such as river discharge, that affect the width and strength of the subtidal surface outflow.

For every transect, subtidal horizontal convergence was observed in the across-channel velocities, especially over the right (looking towards the bay) side of the channel. Subtidal velocity vectors in Figure 14 provide one example of this convergence and its location over both sides of the channel, especially along Transect 2. From subtidal velocity vector plots at successive depths (not shown), it was evident that much of the strong, subsurface horizontal convergence was caused by differences in how the surface outflow rotated with depth to subsurface inflow over the channel relative to the adjacent shoals. Locally, outflow rotated to inflow at a shallower depth over the channel than over the shoals, producing horizontal convergence near the shoulders of the channel, most frequently over the right shoulder (looking into the bay). Over the left shoulder of the channel, horizontal convergence was also affected by the subtidal surface inflow along the coast, which acted either to increase or decrease convergence at different depths, depending on the direction of flow over the channel. Another interesting local feature of the subtidal velocity was that surface outflow consistently rotated anticyclonically with depth to subsurface inflow, thereby producing a vertical structure in the velocity field that emulated an Ekman spiral.

Mean salinity was calculated from the subtidal salinity data and ranged from 25.7 at Transect 1 to 28.5 at Transect 3. Subtidal volume and normalized salinity transports were calculated across each transect, using the subtidal along-channel velocity and salinity fields (Table 1). Net volume transport was consistently into the bay (or toward the bay mouth for Transects 2 and 3). The net northwestward volume and salinity transports across Transects 2 and 3 were consistent with northward flow of shelf water driven by direct frictional coupling of the southerly winds along the shelf. Across the bay mouth (Transect 1), most transport in and out of the bay occurred over Chesapeake Channel (92% of inflow and 57% of outflow), with weaker inflow and outflow (and a small net outflow) over the shoal, and a net outflow over North Channel (Figure 15). Inflows and outflows were separated vertically over the deep channel, but horizontally over the shoal. Net salinity transport (normalized by the sectionally averaged salinity) into the bay was calculated to be $1.36 \times 10^4$ $m^3/s$, which is the first available estimate of this transport for the Chesapeake Bay mouth.

# Table 1

Salinity transports:
($m^3/s \times 10^3$)

| | In | Out | Net | Mean Salinity |
|---|---|---|---|---|
| Transect 1 | 18.6 | -5.6 | 13.6 | 25.7 |
| Transect 2 | 20.5 | -2.9 | 17.6 | 27.2 |
| Transect 3 | 28.4 | -0.3 | 28.1 | 28.5 |

Volume transports:
($m^3/s \times 10^3$)

| | | | |
|---|---|---|---|
| Transect 1 | 17.3 | -5.5 | 11.8 |
| Transect 2 | 19.7 | -3.0 | 16.7 |
| Transect 3 | 27.6 | -0.3 | 27.3 |

Salinity and volume transports. Salinity transports have been normalized by the mean salinity for each transect cross-section, which are also given in the upper table. Positive values indicate transport into (or toward) the bay, while negative values indicate transport out of (or away from) the bay.

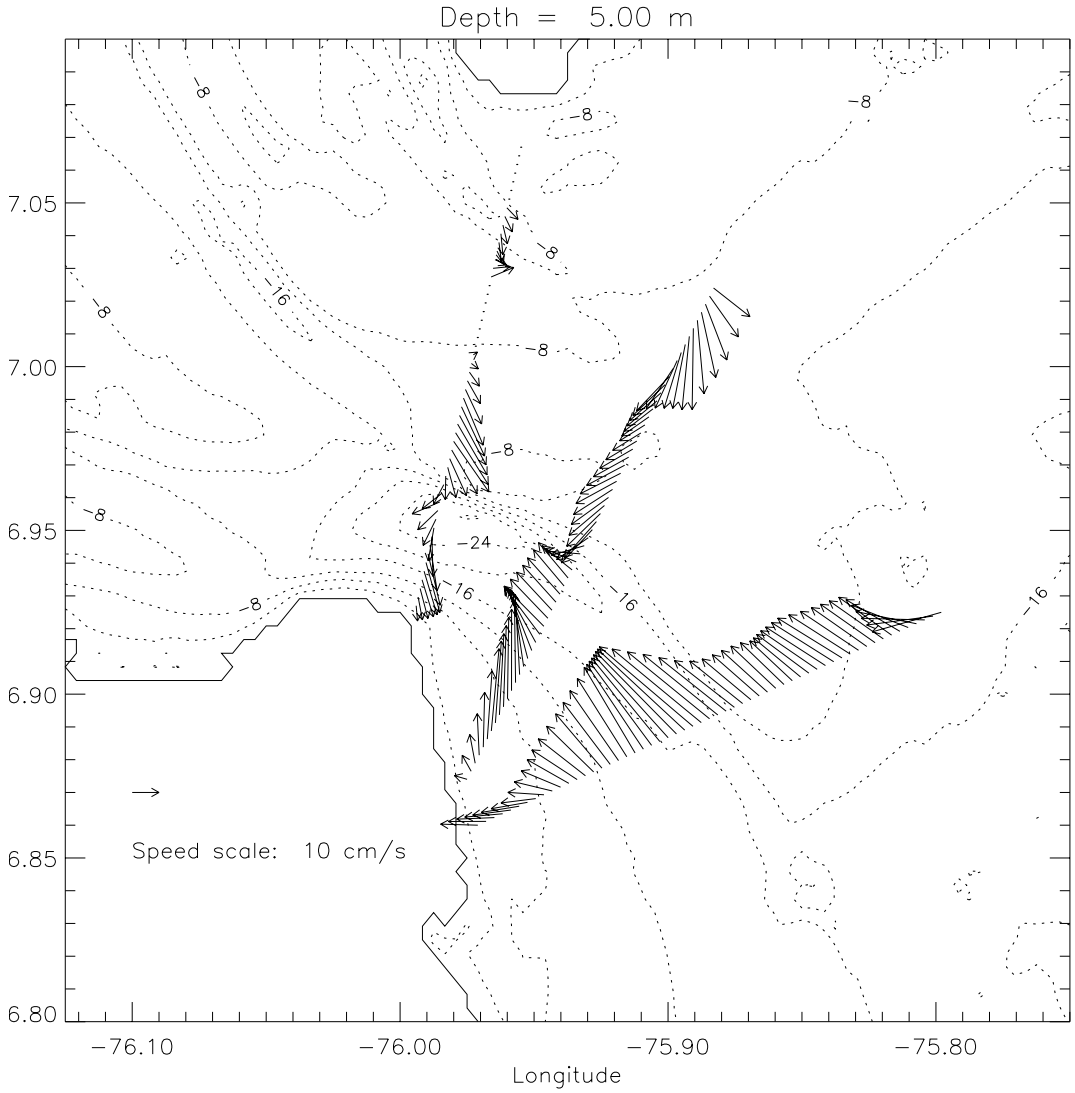


Figure 14. Subtidal velocity vectors at 5 m depth along Transects 1-3. Note that the data used to calculate the subtidal velocities along each transect came from successive 25-hour periods and were therefore not synoptic.

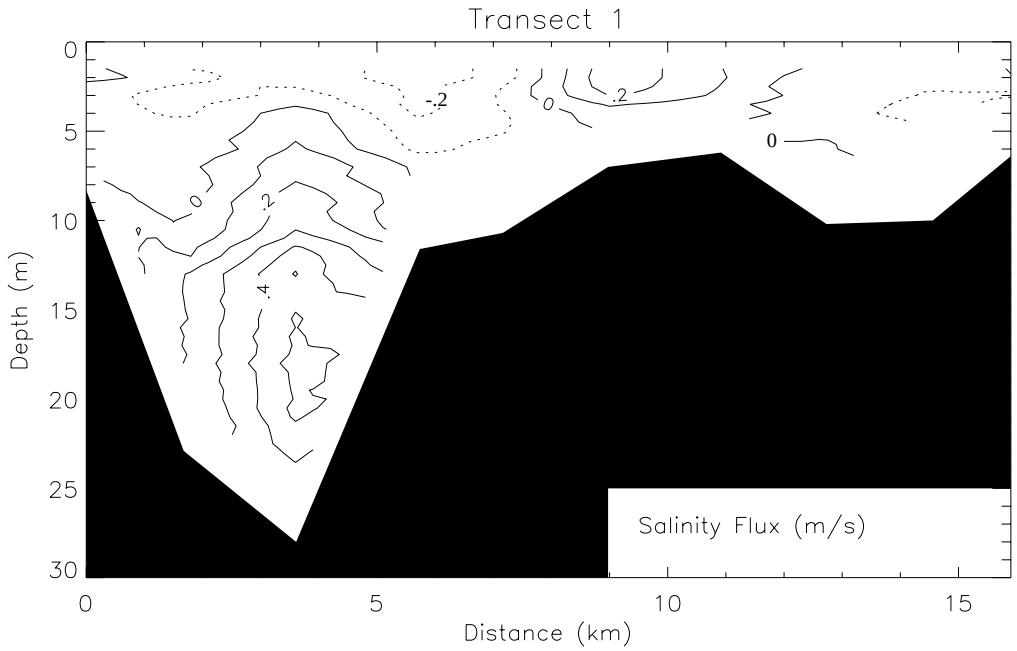


Figure 15. Salinity flux along Transect 1 (Chesapeake Bay mouth), normalized by the mean salinity for the cross-section (<u><$s_n$>). Plot is drawn looking into the bay and contour intervals are 0.1 m/s. Positive (negative) values are plotted as solid (dashed) lines and indicate flux into (out of) the bay.

## SUMMARY

This study described the spatial (horizontal and vertical) and temporal variability of salinity and velocity fields in the Chesapeake Bay plume region under high freshwater discharge and moderate wind forcing conditions. The observed complex vertical and lateral patterns in the fields were explained by interaction between the multiple forces (tidal, gravitational, wind and inertial) affecting circulation in the area, as modified by the channel/shoal bathymetry and coastline morphology. Interesting features in the subtidal circulation that merit further investigation include a surface anticylonic gyre in the northern portion of the bay entrance, a surface anticyclonic gyre to the south of the mouth, and persistent horizontal velocity convergence over the channel shoulders. The smaller-scale transient and subtidal hydrographic and circulation features described in this study may help explain variability in processes, such as larval recruitment, that are sensitive to the structure of the density, salinity and flow fields at the bay mouth. The location, timing and persistence of these features may therefore have a significant impact on processes such as larval recruitment and pollutant dispersal. Future high-resolution sampling of the Chesapeake Bay mouth and plume region, under different wind and freshwater discharge conditions from those of this study, will help to refine our understanding of the effects of these forces on estuary-shelf exchange in this dynamic area.

## ACKNOWLEDGMENTS

This work was mainly funded by the U.S. Mineral Management Service under Cooperative Agreement No. 14-35-001-30807. It was also sponsored in part by the NOAA Office of Sea Grant, under Grant No. NA56RG0489 to the Virginia Graduate Marine Science Consortium and Virginia Sea Grant College Program. Ship time on the NOAA ship *Ferrel* was provided by the National Sea Grant College Program. We greatly appreciate the professional support and cooperation from the crew of the *Ferrel* under the able command of LCDR S.D. McKay. K. Bosley from the NOAA National Ocean Service (NOS) provided the sea level and meteorological data. We also appreciate the technical support of R.C. Kidd and the participation of S. Paraso, E. Haskell, J. Koziana, M. Moore, S. Wathanaprida, and B. Wheless on the cruise.

## REFERENCES

Boicourt, W. C. (1981) Circulation in the Chesapeake Bay entrance region: estuary-shelf interaction. In: *Chesapeake Bay Plume Study: Superflux 1980, NASA Conference Publication 2188*, J.Campbell and J.Thomas, editors, Hampton, VA, pp.61-78.

Boicourt, W. C., S. Y. Chao, H. W. Ducklow, P. M. Gilbert, T. C. Malone, M. R. Roman, L. P. Sanford, J. A. Fuhrman, C. Garside and R. W. Garvine (1987) Physics and microbial ecology of a byoyant estuarine plume on the continental shelf. *Transactions of the American Geophysical Union*, 68, 666-668.

Browne, D. R. and C. W. Fisher (1988) Tide and tidal currents in the Chesapeake Bay. *NOAA Technical Report NOS OMA 3*, Rockville, MD, 84 pp.

Geyer, W. R. and R. Signell (1990) Measurements of tidal flow around a headland with a shipboard acoustic doppler current profiler. *Journal of Geophysical Research*, 95, 3189-3197.

Goodrich, D. M. (1987) Nontidal exchange processes at the Chesapeake Bay entrance. In: *Hydraulic Engineering 1987*, R. Ragan, editor, American Society of Civil Engineers, New York, pp. 493-498.

Goodrich, D. M. (1988) On meteorologically induced flushing in three U. S. East Coast estuaries. *Estuarine, Coastal & Shelf Science*, 26, 111-121.

Haskell, A., A. Valle-Levinson and K. M. M. Lwiza. On the influence of estuarine outflow and bathymetry on semidiurnal tidal currents. Submitted to *Continental Shelf Research*.

Jay, D. A. and J. D. Smith (1990) Circulation, density distribution and neap-spring transitions in the Columbia River Estuary. *Progress in Oceanography*, 25, 81-112.

Johnson, D. F. and K. W. Hess (1990) Numerical simulations of blue crab larval dispersal and recruitment. *Bulletin of Marine Science*, 46, 195-213.

Klinger, B. A. (1994) Inviscid current separation from rounded capes. *Journal of Physical Oceanography*, 24, 1805-1811.

Li, C. and J. O'Donnell (1997) Tidally driven residual circulation in shallow estuaries with lateral depth variation. *Journal of Geophysical Research*, in press.

Lwiza, K. M. M., D. G. Bowers, and J. H. Simpson (1991) Residual and tidal flow at a tidal mixing front in the North Sea. *Continental Shelf Research*, 11, 1379-1395.

Paraso, M. C. and A. Valle-Levinson (1996). Atmospheric forcing effects on sea level and water temperature in the lower Chesapeake Bay: 1992. *Estuaries*, 19, 548-561.

Sanders, T. M. and R. W. Garvine (1996). Frontal observations of the Delaware Coastal Current source region. *Continental Shelf Research*, 16, 1009-1021.

Simpson, J. H., J. Brown, J. P. Matthews, and G. Allen (1990). Tidal straining, density currents and stirring in the control of estuarine circulation. *Estuaries*, 12, 125-132.

Valle-Levinson, A. and J. O'Donnell (1996). Tidal interaction with buoyancy-driven flow in a coastal plain estuary. In: *Coastal and Estuarine Studies, Vol. 53*, American Geophysical Union, pp. 265-281.

Valle-Levinson, A. and K. M. M. Lwiza (1995). The effects of channels and shoals on exchange between the Chesapeake Bay and the adjacent ocean. *Journal of Geophysical Research*, 100, 18551-18563.

Valle-Levinson, A. and K. M. M. Lwiza. Observations on the influence of downwelling winds on the Chesapeake Bay outflow. Submitted to *Proceedings of the 8th International Biennial Conference on Physics of Estuaries and Coastal Seas*.

Valle-Levinson, A., C. Li, T.C. Royer, and L.P. Atkinson. Flow patterns at the Chesapeake Bay entrance. Submitted to *Continental Shelf Research*.

Valle-Levinson, A., J. M. Klinck and G. H. Wheless (1996). Inflows/outflows at the transition between a coastal plain estuary and the coastal ocean. *Continental Shelf Research*, 16, 1819-1847.

Wheless, G. H. and A. Valle-Levinson (1996). A modeling study of tidally driven estuarine exchange through a narrow inlet onto a sloping shelf. *Journal of Geophysical Research*, 101, 25675-25687.